Supporting Information

Bhate and McDermott 10.1073/pnas.1211900109

SI Text

SI Materials and Methods. ***Measurement of the chemical shift anisotropy (CSA).*** The chemical shift tensors for the side chains of E71 and D80 were measured using a CC-2D correlation experiment with 25 ms of dipolar-assisted rotational resonance (DARR) mixing at slow magic-angle spinning (MAS). The optimal spinning rate was found to be 5.555 KHz. This MAS rate prevented overlap between the arginine side chain (approximately 156 ppm) and the Cβ–Cγ/Cδ cross-peaks of interest. It also allowed for a rotor-synchronized dwell time. Spectra were collected at a set temperature of 240 K, which corresponds to a sample temperature of approximately −5 to 0 °C at slow MAS. A modified SPINAL64 (1) decoupling sequence (phases = 12°, 4°, 8°) was used based on empirical optimization of the signal. The data were acquired over approximately 4 d of signal averaging on a 750-MHz instrument using a 4-mm HXY probe. The data were acquired with the receiver in analog mode to minimize baseline artifacts at the large sweepwidths.

Data analysis. An example of a region of the 2D DARR spectrum is shown in panel A of Fig. S3 together with the sideband profile for E71 extracted from the data. The center band and sidebands of the peaks of interest were picked using our assignments of E71 and D80. Additionally, two other "control" peaks were used to validate our method on KcsA. E51, a solvent, exposed and definitely deprotonated carboxyl and the backbone carbonyl of A32, which is a classical α-helical alanine. Both the intensity and the integral of the peak were computed using both Sparky and NMRDraw to get a sense of the error. These values were all in good agreement with each other. The peak intensities were fit in SPINEVOLUTION (2) to extract the asymmetry and anisotropy parameters of the chemical shift tensors. The fitting routine was validated by performing the same experiment on the carboxyl group of crystalline glycine to extract its chemical shift tensor. Additionally, the tensor parameters extracted for the backbone carbonyl group of A32 agree very well with previous measurements of helical alanine tensors (3). Errors in the chemical shift tensor were determined by evaluating the fit using a t distribution at the 95% confidence level. The reconstructed sideband patterns for A32 and E51 are shown in Fig. S3.

1. Fung BM, Khitrin AK, Ermolaev K (2000) An Improved broadband decoupling sequence for liquid crystals and solids. *J Magn Reson* 142:97–101.
2. Veshtort M, Griffin R (2006) SPINEVOLUTION: A powerful tool for the simulation of solid and liquid state NMR experiments. *J Magn Reson* 178:248–282.
3. Wylie BJ, et al. (2007) Chemical-shift anisotropy measurements of amide and carbonyl resonances in a microcrystalline protein with slow magic-angle spinning NMR spectroscopy. *J Am Chem Soc* 129:5318–5319.

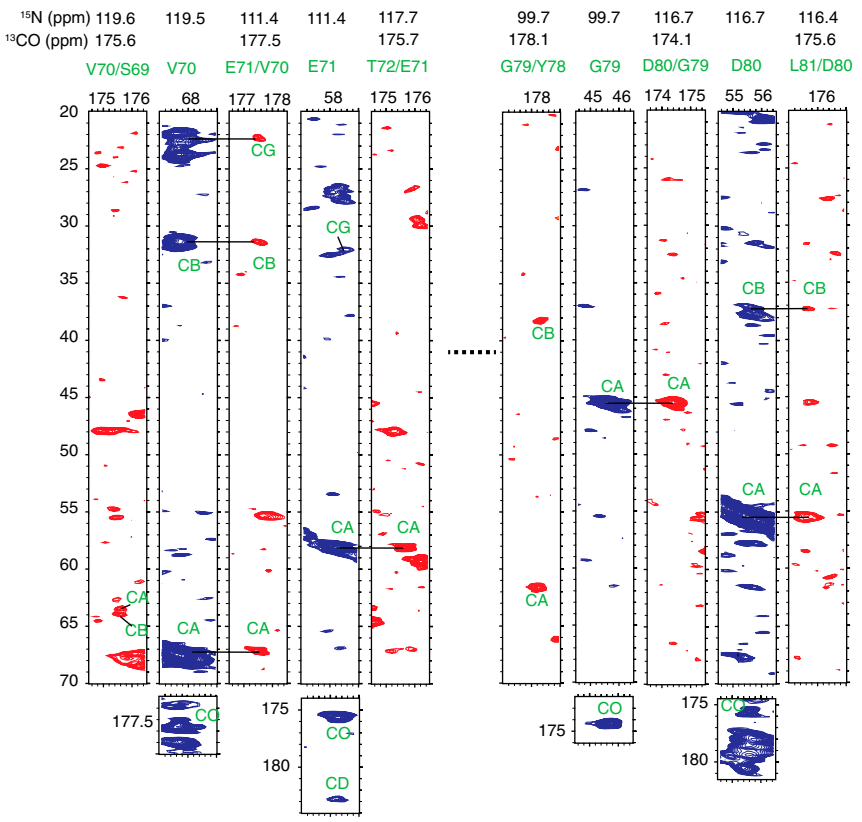

Fig. S1. Sequential assignments for residues S69-T72 and Y78-L81 that surround the selectivity filter are shown as a strip plot. The plot shows amide nitrogen planes of the 3D NCOCX (red) and NCαCX (blue) experiments and illustrates the backbone and side-chain assignment of the key pore residues E71 and D80, which share a hydrogen bond. Sequential correlations for other residues in the selectivity filter have been published previously by our group (1) and by the Baldus and coworkers (2). Our assignment is further validated by the CC-2D spectrum of the mutant KcsA–E71A that showed one missing glutamic acid spin system whose shifts corresponded to those assigned to E71 from the 3D. The mutant alanine is also detected as an extra peak in the alanine Cα–Cβ region.

1 Bhate MP, Wylie BJ, Tian L, McDermott AE (2010) Conformational dynamics in the selectivity filter of KcsA in response to potassium ion concentration. *J Mol Bio* 401:155–166.
2 Schneider R, et al. (2008) Solid-state NMR spectroscopy applied to a chimeric potassium channel in lipid bilayers. *J Am Chem Soc* 130:7427–7435.

A

		E71A minor	E71A major	WT high K+	1K4C SPARTA+	2ATK SPARTA+
W67	CB	29.9	29.5	29.5	29.6	29.4
W67	CG	110.9	111.6	111	NA	NA
T74	CA	61.5	60.8	61.1	62	61.2
T74	CB	69.2	69.9	69.7	69.5	68.5
Y78	CA	60.7	61.5	61.5	60.7	56.3
Y78	CB	38.8	38.3	38.3	39	40.3
D80	CA	55.8	55.8	55.5	56	52.5
D80	CB	35.5	36.1	37.3	41.1	40.5

B

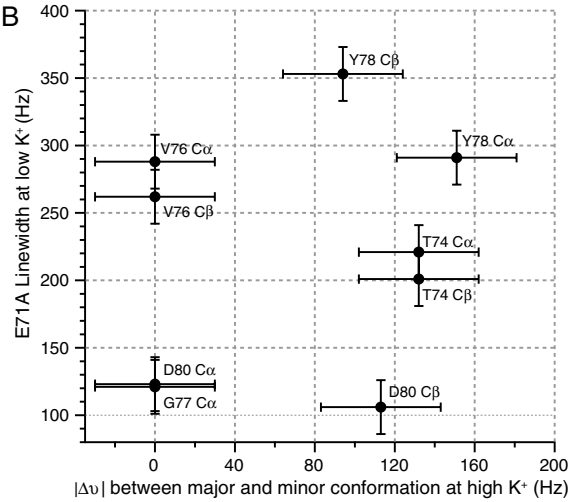

Fig. S2. (*A*) Chemical shift analysis of the major and minor conformations observed in NMR spectra of the mutant E71A at sites W67, T74, Y78, and D80 is shown. Of the two conformations, the major conformation is very similar to the previously characterized WT conductive state of the filter (PDB 1K4C). The minor conformation may be the "flipped" state, previously reported as being observed in a small percent of crystals. However, the large error bars in current state-of-the-art chemical shift prediction programs preclude any definitive confirmation of this point. (*B*) A plot of the NMR linewidth of key residues in the selectivity filter of the E71A mutant at low K^+ versus the observed chemical shift differences between the major and minor conformations of the mutant filter at high K^+. There is no obvious correlation between the extent of the line broadening observed at low K^+ and the distribution of chemical shifts at high K^+. This rules out the possibility that the broadening at low K^+ is the same process as the slow exchange into multiple conformations observed at high K^+. We speculate that this extra linewidth in the mutant at low potassium could be caused by one of two processes. First, disrupting the E71–D80 hydrogen bond could compromise the tetrameric stability of the mutant channel at low potassium much more than the WT channel, so what we observe for the mutant at low potassium is actually the KcsA monomer with a distribution of selectivity filter conformations, and not the tetramer. Second, it is possible that because of the reduced steric constraints, the mutant channel exhibits disorder or dynamics at low potassium that affect the solid-state NMR lineshape. Distinguishing between these hypotheses is complicated, but it is worthwhile to note that the E71A mutant tetramer is less stable than the WT.

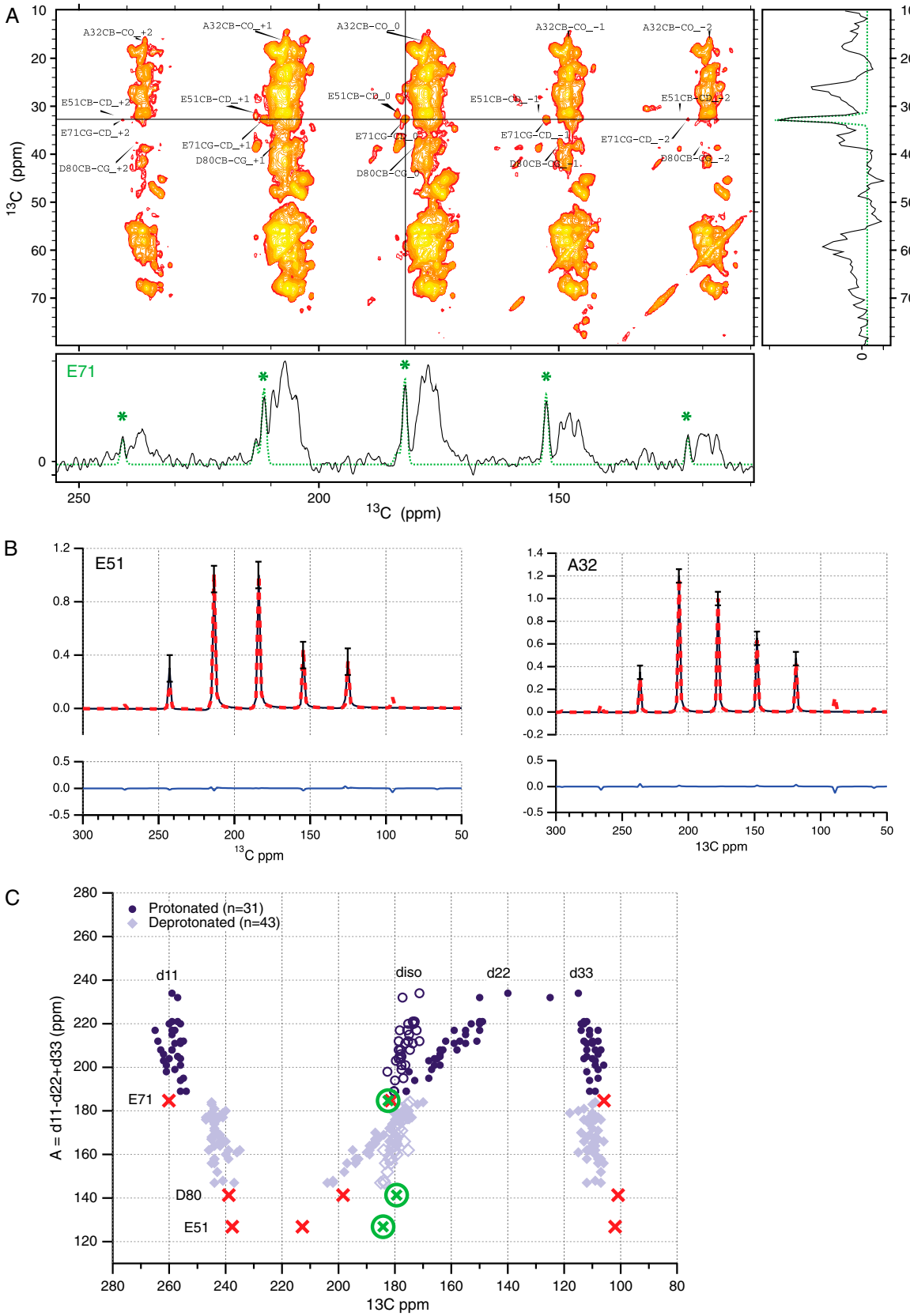

Fig. S3. (*A*) A section of the slow-MAS CC-2D spectrum of KcsA is shown. The center band (0) and the sidebands (+2, +1, −1, −2) for four residues (E71, D80, A32, and E51) are labeled. The slices show the extracted intensities for the sideband manifold for the E71 carboxyl. (*B*) The reconstructed sideband manifolds for the control peaks: A32 backbone carbonyl (*Left*) and the E51 side-chain carboxyl (*Right*) are shown. Experimental data are shown in black, the best fit is in red, and the residual is shown underneath in blue. (*C*) A graphical representation of the tensor parameters for E71, D80, and E51 compared to values from a database of model compounds (1). A parameter called $A(=\delta 11-\delta 22+\delta 33)$ is plotted against the individual values for the tensor components for

31 protonated (dark blue, filled) and 43 deprotonated (light blue, filled) compounds. The isotropic shifts are indicated by open markers. Note that δ11 is known to be the best indicator of protonation, δ22 is a measure of the strength of the hydrogen bond associated with the carbonyl side of the carboxyl, and δ33 is essentially invariant with protonation.

1 Gu Z, Zambrano R, McDermott A (1994) Hydrogen bonding of carboxyl groups in solid-state amino acids and peptides: Comparison of carbon chemical shielding, infrared frequencies, and structures. *J Am Chem Soc* 116:6368–6372.

2 Gu Z, McDermott A (1993) Chemical shielding anisotropy of protonated and deprotonated carboxylates in amino acids. *J Am Chem Soc* 115:4282–4285.

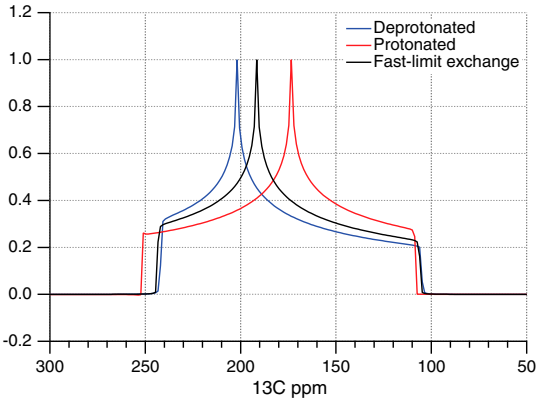

Fig. S4. Simulations of a static CSA lineshape of a typical protonated glutamic acid carboxyl (δ11 = 252, δ22 = 174, δ33 = 109; red); a typical deprotonated glutamic acid carboxyl (δ11 = 242, δ22 = 202, δ33 = 105; blue); and a fast-limit equal-population average of the two (δ11 = 243.5, δ22 = 191.5, δ33 = 107; black), taking into account the 30-degree reorientation of the δ11 and δ22 axes in the plane of the carboxyl group, upon protonation. The results show that a fast-limit average of the two tensors, which is what we would expect for a low-barrier hydrogen bond, still retains some asymmetry in the lineshape, which is inconsistent with our data on E71 and D80.

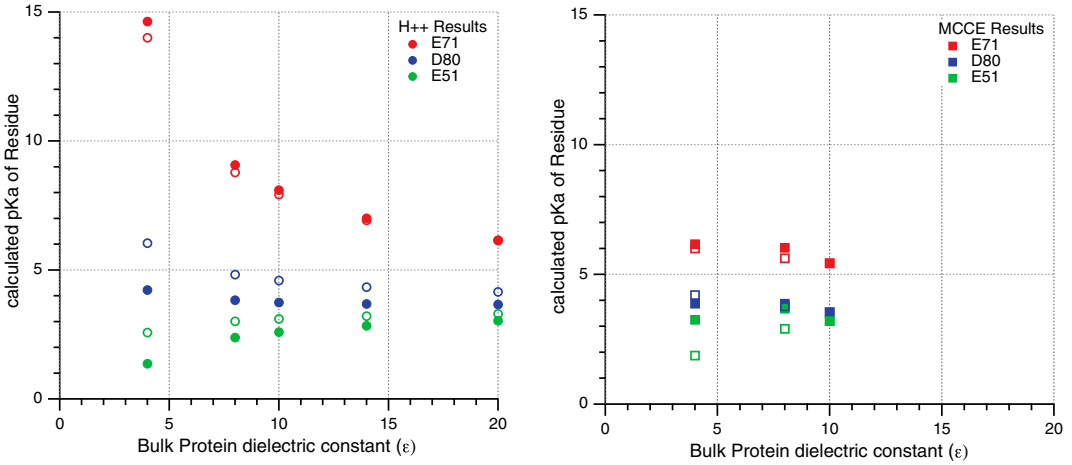

Fig. S5. Electrostatic calculations of pK_a of KcsA at high K^+, and pH 7.5, based on the coordinates from the high-resolution published crystal structures 1K4C (filled) and 1K4D (open). We used two different programs, H + + (*Left*) (1) and MCCE (*Right*) (2), to calculate the pK_a of E71 (red), D80 (blue), and E51 (green) for a range of different bulk protein dielectric constants. The calculations suggest two results: (*i*) The pK_a of E71 is elevated above D80, so a shared proton would preferentially reside at E71; and (*ii*) there is no significant change in the pK_a of E71 between the conductive and collapsed states of the channel.

1 Gordon J, et al. (2005) H++: A server for estimating pK_as and adding missing hydrogens to macromolecules. *Nucleic Acids Res* 33:W368–W371.

2 Georgescu RE, Alexov E, Gunner MR (2002) Combining conformational flexibility and continuum electrostatics for calculating pK_as in proteins. *Biophys J* 83:1731–1748.

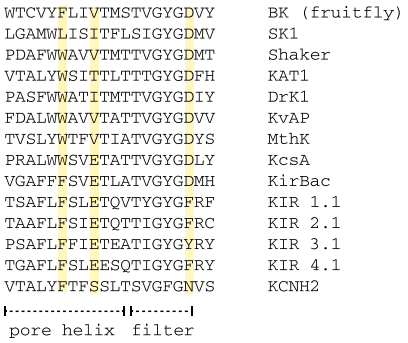

Fig. S6. Sequence alignment of KcsA with various other potassium channels. Across all these different channels, at least one of the hydrogen bond pairs in the pore helix is conserved.

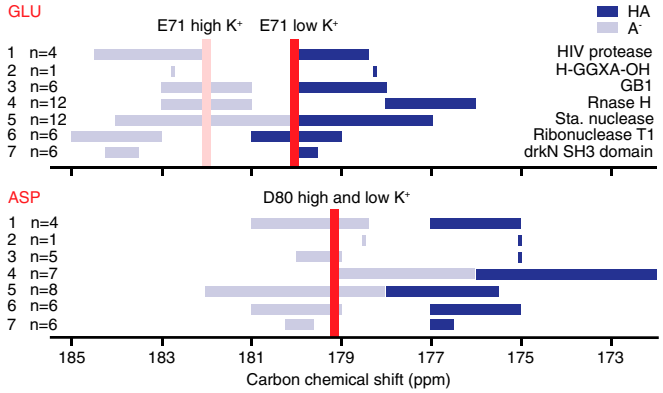

Fig. S7. A summary of the side-chain carboxyl chemical shift distributions for glutamic and aspartic acid sites reported in the literature (1–7). The deprotonated shift range is shown in light blue and the protonated shift range is shown in dark blue for glutamic acid residues (*Top*) and aspartic acid residues (*Bottom*). Our measured shifts for E71 and D80 are marked in red. The data show that, based on the literature, isotropic carboxyl chemical shifts for E71 and D80 at high potassium correspond to the deprotonated states for both these side chains.

1 Yamazaki T, et al. (1994) NMR and X-ray evidence that the HIV protease catalytic aspartyl groups are protonated in the complex formed by the protease and a non-peptide cyclic urea-based inhibitor. *J Am Chem Soc* 116:10791–10792.

2 Schmidt HLF, Shah GJ, Sperling LJ, Rienstra CM (2010) NMR determination of protein pK(a) values in the solid state. *J Phys Chem Letts* 1:1623–1628.

3 Castañeda C, et al. (2009) Molecular determinants of the pKa values of Asp and Glu residues in staphylococcal nuclease. *Proteins* 77:570–588.

4 Oda Y, et al. (1994) Individual ionization constants of all the carboxyl groups in ribonuclease HI from *Escherichia coli* determined by NMR. *Biochemistry* 33:5275–5284.

5 Tollinger M, Forman-Kay JD, Kay LE (2002) Measurement of side-chain carboxyl pK(a) values of glutamate and aspartate residues in an unfolded protein by multinuclear NMR spectroscopy. *J Am Chem Soc* 124:5714–5717.

6 Spitzner N, et al. (2001) Ionization properties of titratable groups in ribonuclease T 1. *Eur J Biophys* 30:186–197.

7 Richarz R, Wüthrich K (1978) Carbon-13 NMR chemical shifts of the common amino acid residues measured in aqueous solutions of the linear tetrapeptides H-Gly-Gly- X-L- Ala-OH. *Biopolymers* 17:2133–2141.

Table S1. Hydrogen bonding distances* in the conductive state of the selectivity filter of KcsA enumerated corresponding to the geometries in Fig. 1

		Conductive filter (1K4C) (Å)	Collapsed filter (1K4D) (Å)	Inference re: protonation
E71 Cδ–O_1	H_2O #1	2.8	2.8	Because E71 Cδ–O_1 is accepting from
"	Y78 N–H	3.0	5.8	both water and N–H, it must be
"	D80 Cγ–O_1	3.4	3.3	the carbonyl end of the side chain
"	D80 Cγ–O_2	4.9	4.2	
"	W67 Nε	4.9	3.9	
E71 Cδ–O_2	D80 Cγ–O_1	2.6	2.5	Unclear—either E71 Cδ–O_2 or D80 Cγ–O_1
"	W67 Nε	3.2	3.3	must be protonated
"	D80 Cγ–O_2	3.5	3.5	
"	H_2O #1	3.5	3.6	
D80 Cγ–O_1	E71 Cδ–O_2	2.6	2.5	Unclear, but given the proximity to
"	D80 N-H	2.7	2.6	D80 N–H, possibly deprotonated
"	H_2O #1	3.1	3.1	
"	E71 Cδ–O_1	3.4	3.3	
D80 Cγ–O_2	H_2O #2	2.6	3.2	D80 Cγ–O_2 seems essentially solvated
"	W67 Nε	3.0	3.3	and probably not protonated
"	E71 Cδ–O_2	3.5	3.5	
"	E71 Cδ–O_1	4.9	4.2	

The hydrogen bond network around E71 suggests that either E71 or D80 must be protonated to avoid electrostatic repulsion. Because D80 is closer to the solvent, it is more likely that E71 bears the proton. However, this conclusion is inferential because protons are not visible at the resolution of the structures. The data also show that the biggest change occurs because of breaking of a contact between E71 and Y78.
*The distances were measured in Pymol using the deposited structures 1K4C and 1K4D (1).

1 Zhou Y, Morais-Cabral JH, Kaufman A, Mackinnon R (2001) Chemistry of ion coordination and hydration revealed by a K channel Fab complex at 2.0A resolution. *Nature* 414:43–48.

Table S2. Assignment of E71 and D80

	N	CO	CA	CB	CG	CD
E71						
Our assignment*	111.4†	175.6	58.3	27.5	32.3	182.5
Ader et al. (1)	N/A	N/A	58.2	27.1	32.5	181.9
Chill et al. (2)	N/A	180.1	N/A	N/A	N/A	N/A
SHIFTX2	117.2	176.3	58.2	28.9	30.7	176.4
SPARTA+	120.2	176.0	56.9	29.7	N/A	N/A
D80						
Our assignment*	116.7	175.5	55.5	37.3	179.3	—
Ader et al. (1)	118.4	N/A	55.7	37.3	179.4	—
Chill et al. (2)	115.7	N/A	N/A	N/A	N/A	—
SHIFTX2	118.31	175.1	54.4	40.7	174.6	—
SPARTA+	120.9	176.4	54.5	40.6	N/A	—

*Our assignment is further validated by (*i*) its agreement with previously reported chemical shifts for these residues from Baldus and coworkers (Kv1.2–KcsA chimera in asolectin liposomes) (1) and Bax and coworkers (WT-KcsA in SDS micelles) (2), and (*ii*) its general agreement with the predicted chemical shifts from SPARTA+ (3) and SHIFTX2 (4).
†The observed nitrogen shift (111.4 ppm) for E71 is much lower than expected. However, it is well within 3σ of the average helical backbone nitrogen shift for glutamic acids reported in the Biological Magnetic Resonance Data Bank, and there are over 50 reported instances of glutamic acid nitrogens in the range of 110–112 ppm.

1 Schneider R, et al. (2008) Solid-state NMR spectroscopy applied to a chimeric potassium channel in lipid bilayers. *J Am Chem Soc* 130:7427–7435.
2 Chill JH, Louis JM, Miller C, Bax A (2006) NMR study of the tetrameric KcsA potassium channel in detergent micelles. *Protein Sci* 15:684–698.
3 Shen Y, Bax A (2010) SPARTA+: A modest improvement in empirical NMR chemical shift prediction by means of an artificial neural network. *J Biomol NMR* 49:1–10.
4 Han B, Liu Y, Ginzinger SW, Wishart DS (2011) SHIFTX2: Significantly improved protein chemical shift prediction. *J Biomol NMR* 50:43–57.

Table S3. Solvent accessibility for E71 and D80 calculated using the standard crystal structures 1K4C (high K^+) and 1K4D (low K^+) with VADAR* (1)

Residue number	Residue name	Fractional accessible surface area of side chain† (1K4C|1K4D)
71	GLU	0.03|0.07
72	THR	0.09|0.14
73	ALA	0.02|0.02
74	THR	0.35|0.38
75	THR	0.55|0.59
76	VAL	0.49|0.39
77	GLY	0.60|0.78
78	TYR	0.58|0.55
79	GLY	0.50|0.65
80	ASP	0.53|0.53

*From the Wishart group (http://vadar.wishartlab.com/).

†The values range from 0 (not at all solvent accessible) to 1 (completely solvent accessible).

1 Willard L, et al. (2003) VADAR: A web server for quantitative evaluation of protein structure quality. *Nucleic Acids Res* 31:3316–3319.